EPJ Web of Conferences **95**, 04077 (2015)
DOI: 10.1051/epjconf/20159504077

B physics and quarkonia at CMS

Claudia-Elisabeth Wulz[1,a], on behalf of the CMS Collaboration

[1]Institute of High Energy Physics of the Austrian Academy of Sciences,
Nikolsdorfergasse 18, A-1050 Vienna, Austria

Abstract. Selected recent results on B physics and quarkonia are presented. These include a determination of the CP-violating phase ϕ_s and the decay width difference $\Delta\Gamma_s$ of the light and heavy B_s states with $B_s \to J/\psi\,\Phi(1020)$, prompt double-differential production cross sections of J/ψ and $\psi(2S)$, and polarization measurements for J/ψ, $\psi(2S)$, $\Upsilon(1S)$, $\Upsilon(2S)$, and $\Upsilon(3S)$. Results are based on proton-proton data recorded at the LHC at centre-of-mass energies of 7 or 8 TeV.

1 Introduction

Heavy flavours are produced abundantly at the LHC. The CMS experiment [1] is well suited to detect them in spite of large backgrounds, due to its excellent track and vertex reconstruction as well as particle identification capabilities.

For the measurement of the CP-violating weak phase ϕ_s and the decay width difference $\Delta\Gamma_s$ of the light and heavy states of B_s mesons a proton-proton sample of $B_s \to J/\psi\,\Phi(K^+K^-)$ corresponding to an integrated luminosity of about 20 fb^{-1} at a centre-of-mass energy of $\sqrt{s} = 8$ TeV has been used. A time-dependent and flavour-tagged analysis of the $\mu^+\mu^-K^+K^-$ final state has been performed.

Heavy quarkonia are probes to understand hadron formation. Until recently their production cross sections have only been measured in the lower p_T range. Furthermore, polarization measurements by different experiments yielded inconclusive results [2]. CMS has studied quarkonium production and polarization with a data sample of about 4.9 fb^{-1} at $\sqrt{s} = 7$ TeV. The production of S-wave quarkonia has been analyzed using their decays into muon pairs, and P-wave quarkonia production has been analyzed through radiative decays. The CMS measurements presented in this report contribute significantly to the understanding of quarkonia polarization and the underlying theoretical scenarios, in particular in the newly accessible high transverse momentum (p_T) range.

An overview of current B physics results of the CMS experiment may be found here: https://twiki.cern.ch/twiki/bin/view/CMSPublic/PhysicsResultsBPH.

2 Measurement of ϕ_s and $\Delta\Gamma_s$ of the light and heavy B_s meson states

The B_s system offers several opportunities to detect possible deviations from the standard model (SM). In this report the measurements of the CP-violating weak phase ϕ_s and the decay width difference $\Delta\Gamma_s$ of the light and heavy B_s mass eigenstates are described. The weak phase ϕ_s arises from interference

[a]e-mail: claudia.wulz@cern.ch

between direct B_s decays into a $c\bar{c}s\bar{s}$ CP eigenstate and decays through B_s-$\bar{B}_s$ mixing into the same final state. Neglecting penguin diagram contributions, ϕ_s is related to the CKM matrix elements, with $\phi_s \approx -2\beta_s$, and $\beta_s = \arg(-V_{ts}V_{tb}^*/V_{cs}V_{cb}^*)$. The SM prediction determined from a global fit to experimental data [3] is $-2\beta_s$ (SM) $= 0.0363^{+0.0016}_{-0.0015}$ rad. The decay width difference is predicted to be $\Delta\Gamma_s = 0.087 \pm 0.021$ ps^{-1}, assuming no new physics in B_s-$\bar{B}_s$ mixing [4].

CMS has performed a time-dependent, flavour-tagged analysis of the $B_s \to J/\psi(\mu^+\mu^-)\,\Phi(K^+K^-)$ final state, with 49000 reconstructed B_s decays at $\sqrt{s} = 8$ TeV [5]. To disentangle the CP-odd and CP-even final states the set of decay angles $\Theta = (\theta_T, \varphi_T, \psi_T)$ has been measured. The angles θ_T and φ_T are the respective polar and azimuthal angles of the μ^+ in the rest frame of the J/ψ, where the x axis is defined by the decay plane of the $\Phi(1020)$ meson in the J/ψ rest frame and the x-y plane is defined by the decay plane of the $\Phi \to K^+K^-$. The helicity angle ψ_T is the angle of the K^+ in the Φ rest frame with respect to the negative J/ψ momentum direction.

The differential decay rate of the $B_s \to J/\psi\,\Phi(1020)$ in terms of proper decay length ct and angular variables can be written as [6]:

$$\frac{d^4\Gamma(B_s(t))}{d\Theta dct} = \sum_{i=1}^{10} O_i(\alpha, ct)\cdot g_i(\Theta), \tag{1}$$

with angular functions $g_i(\theta_T, \varphi_T, \psi_T)$ and time-dependent functions O_i:

$$O_i(\alpha, ct) = N_i e^{-ct/c\tau}[a_i cosh(\frac{1}{2}\Delta\Gamma_s ct) + b_i sinh(\frac{1}{2}\Delta\Gamma_s ct) + c_i cos(\Delta m_s ct) + d_i sin(\Delta m_s ct)]. \tag{2}$$

α is a set of ten physics parameters, including ϕ_s and $\Delta\Gamma_s$. b_i and d_i depend on ϕ_s. The definition of the parameters follows LHCb [7].

Events are selected by trigger algorithms optimized to identify b hadrons through their decay to J/ψ particles originating from secondary vertices. Two muon candidates coming from a common decay vertex are required, each with $p_T(\mu) > 4$ GeV, and $p_T(\mu\mu) > 6.9$ GeV with a dimuon mass window between 2.9 and 3.3 GeV. The transverse decay length significance $L_{xy}/\sigma(L_{xy})$ is required to be greater than three, where L_{xy} is the distance between the primary and secondary vertices in the transverse plane, and $\sigma(L_{xy})$ is its uncertainty.

In the offline selection, tighter cuts including a J/ψ mass constraint $|m_{\mu^+\mu^-} - M_{J/\psi}| < 150$ MeV are applied to the muons, and two kaons with momenta greater than 0.7 GeV and a Φ mass constraint $|m_{K^+K^-} - M_\Phi| < 10$ MeV are also required. The $B_s(\mu\mu KK)$ is reconstructed by a combined kinematic and vertex fit. The mass of the four-particle state must be between 5.24 and 5.49 GeV, and the χ^2 vertex fit probability must be greater than 2%. In case of multiple primary vertices the one closest to the B_s is selected.

The main background comes from non-prompt J/ψ from b hadrons such as B^0 or Λ_b. The lifetime and angular resolution as well as the corresponding measurement efficiencies are determined from simulation. The angular efficiency is modeled by a 3D-function of the decay angles. The angular resolution is not included in the nominal fit, but as a systematic uncertainty. Similarly, the proper decay time efficiency is assumed to be flat in the fitting range from 0.02 to 0.3 cm. Any variations are included as systematic uncertainties. The proper decay time resolution is 70 fs or 21 μm if expressed as a length. Fig.1 shows the distributions of the J/ψKK invariant mass, proper decay length and its uncertainty, respectively.

The flavour of the B_s at production time is determined by tagging the electron or muon from the opposite side B, considering its charge. The tagging performance is optimized by maximizing the tagging power $P_{tag} = \epsilon_{tag}(1-2\omega)^2$ separately for electrons and muons. ω is the mistag fraction and

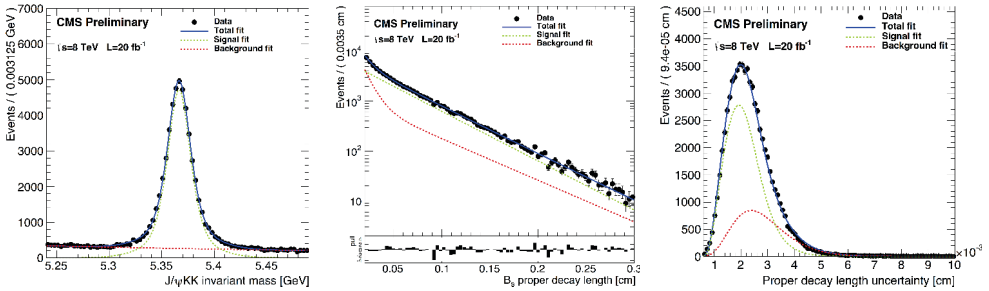

Figure 1. B_s candidate distributions: (Left) invariant mass, (Centre) B_s proper decay length and pull, (Right) B_s proper decay length uncertainty.

ϵ_{tag} the tagging efficiency. The tagging power is calibrated with data, using the channel $B^+ \to J/\psi K^+$, and checked by simulation with $B^+ \to J/\psi K^+$ and $B_s \to J/\psi K^{*0}$ events. The combined average tagging performance is $\omega = 32.3 \pm 0.3\%$, $\epsilon_{tag} = 7.67 \pm 0.04\%$, and $P_{tag} = 0.97 \pm 0.03\%$.

An extended maximum likelihood fit to the data, using the signal model defined in eq. (1) and (2) above is used to extract the parameters, constraining Δm_s to the current world average value of $(17.69 \pm 0.08) \times 10^{12}\ \hbar/s$ in the fit. Information on the invariant mass, proper decay length, and the three decay angles of the reconstructed B_s candidates is included in the fit. From this multidimensional fit the ten parameters described above are determined. Several sources of systematic uncertainties in the physics parameters are considered by testing the assumptions made in the fit model and those associated in the fit procedure. Biases, which could be intrinsic to the fit model itself, are also taken into account.

Fig. 2 shows the angular distributions of the B_s candidates.

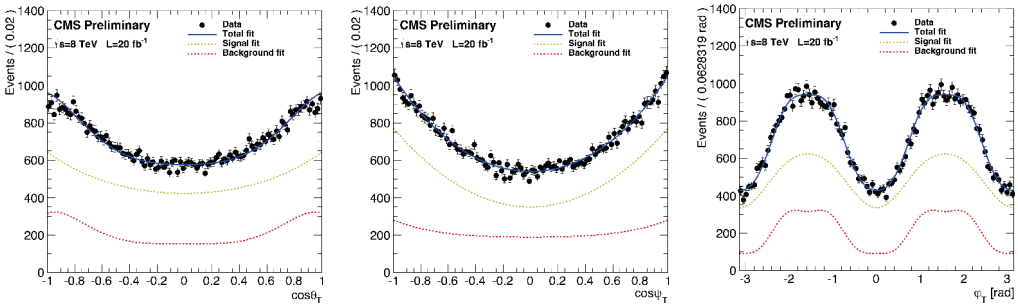

Figure 2. Angular distributions of the B_s candidates. Uncertainties are statistical only.

The measured values for the weak phase and the decay width difference between the B_s mass eigenstates are:

$$\phi_s = -0.03 \pm 0.11\ (\text{stat.}) \pm 0.03\ (\text{syst.})\ \text{rad},$$
$$\Delta\Gamma_s = 0.096 \pm 0.014\ (\text{stat.}) \pm 0.007\ (\text{syst.})\ \text{ps}^{-1}.$$

The CMS contours in the $\Delta\Gamma_s - \phi_s$ plane, results from other experiments and experiment combinations performed by the HFAG group [8] are displayed in Fig. 3.

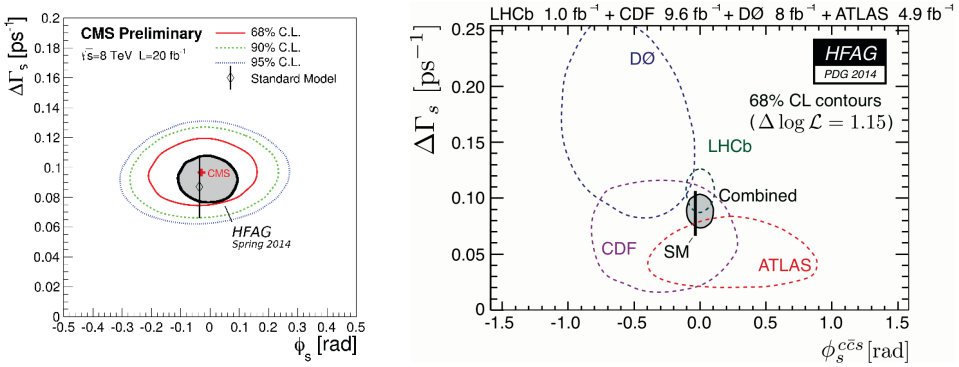

Figure 3. (Left) The 68%, 90% and 95% C.L. contours in the $\Delta\Gamma_s - \phi_s$ plane and the SM prediction, (Right) 68% C.L. contours for different experiments and combination.

3 Measurement of J/ψ and ψ(2S) prompt double-differential cross sections

The production of promptly produced J/ψ and ψ(2S) states has been studied using data samples of dimuons recorded at $\sqrt{s} = 7$ TeV, with integrated luminosities of 4.55 and 4.90 fb^{-1}, respectively [9]. For the first time it was possible to access the transverse momentum range up to the order of 100 GeV. The measurements are based on a two-dimensional analysis of the dimuon invariant mass and pseudo-proper decay length, in the rapidity interval $|y| < 1.2$. No distinction was made between directly produced mesons and those originating from the decay of heavier charmonium states. The feed-down to the J/ψ state from ψ(2S) and χ_c decays is about 8% and 25%, respectively [10].

At the trigger level, opposite-sign dimuons in the invariant mass windows 2.80 – 3.35 GeV or 3.35 – 4.05 GeV are selected. The vertex fit χ^2 probability must be greater than 0.5% and the distance to the beam axis smaller than 5 mm. Prompt charmonia are distinguished from B-hadron decays through the dimuon pseudo-proper decay length $\ell = L_{xy} m_{\psi(nS)}/p_T$, with L_{xy} being the most probable transverse decay length in the laboratory frame, measured after removing the two muon tracks from the calculated primary vertex position [13]. The prompt charmonium yields are evaluated in different $(|y|, p_T)$ bins. The shape of the mass peaks in the signal region is represented by a Crystal Ball function, whereas the continuum background is described by an exponential function. Fig. 4 shows examples of the projections of the dimuon invariant mass and pseudo-proper decay length from the two-dimensional analysis in a particular $(|y|, p_T)$ bin, for the ψ(2S) case.

Systematic uncertainties are evaluated by repeating the two-dimensional fit with different functional forms. They are negligible at low p_T and increase to about 2% for the J/ψ and 6% for the ψ(2S) in the highest-p_T bins. Muon detection efficiencies are measured by a tag-and-probe technique, using event samples recorded with triggers specially designed for this purpose. At high p_T, the two muons may be emitted close to each other, and the efficiency of the dimuon trigger is different from the product of the two single-muon efficiencies so that it has to be multiplied by a scale factor ρ determined by Monte Carlo simulations.

In Fig. 5 the single-muon detection efficiencies, the ρ parameter, and the acceptances for different polarization scenarios are shown for J/ψ events. For the cross section measurements an unpolarized scenario has been assumed. This assumption is well justified, as shown in the next section.

Results on the double-differential J/ψ and ψ(2S) production cross sections in various rapidity bins, multiplied by the corresponding branching fractions, are given in Fig. 6. The cross section

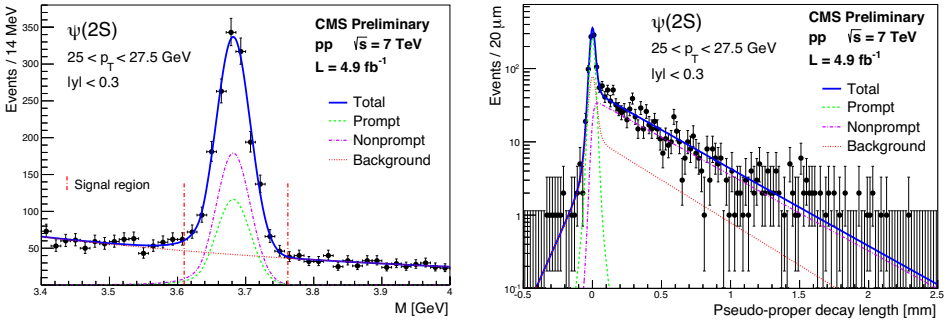

Figure 4. Projections of the (Left) dimuon invariant mass, (Right) pseudo-proper decay length for $\psi(2S)$ events. The curves represent the results of the fits.

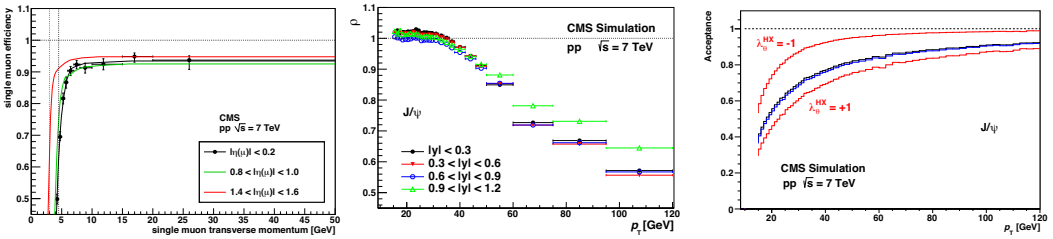

Figure 5. (Left) Single muon detection efficiencies, (Centre) Scale factor ρ reflecting muon correlations, (Right) Acceptances for different polarization scenarios in the centre-of-mass helicity frame.

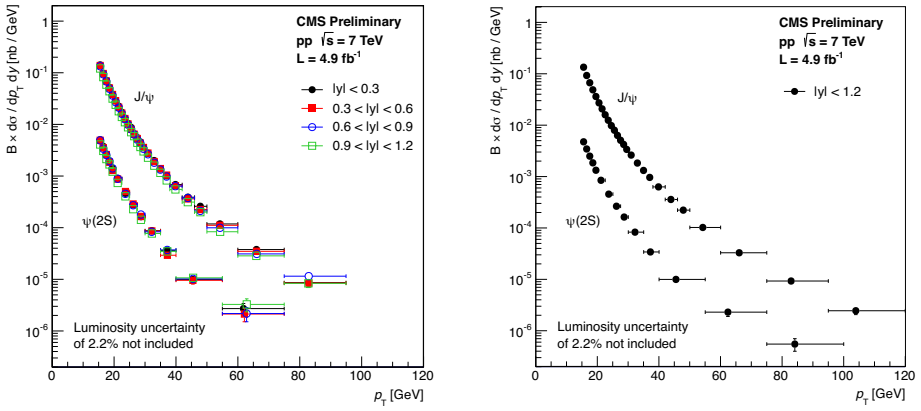

Figure 6. Double-differential cross sections for J/ψ and ψ(2S), as functions of p_T in different rapidity regions.

measurement in the broad rapidity range $|y| < 1.2$ allows for particularly interesting comparisons with theoretical models in the high-p_T range, which has not been probed so far.

4 Measurement of the polarization of S- and P-wave quarkonia

The polarization of $J^{PC} = 1^{--}$ vector quarkonium states has been measured through the angular distributions of dimuons from their decay. The most general form of this distribution can be written as [14]

$$\frac{dN}{d\Omega} \propto \frac{1}{1+3\lambda_\vartheta}(1+\lambda_\vartheta \cos^2\vartheta + \lambda_\varphi \sin^2\vartheta \cos^2 2\varphi + \lambda_{\vartheta\varphi} \sin 2\vartheta cos\varphi), \tag{3}$$

where ϑ and φ are the polar and azimuthal angles, respectively, of the μ^+ with respect to the chosen polarization frame. The angular distribution parameters $\lambda_\vartheta, \lambda_\varphi, \lambda_{\vartheta\varphi}$ are different in different polarization frames. A frame-independent parameter is given by $\tilde{\lambda} = (\lambda_\vartheta + 3\lambda_\phi)/(1-\lambda_\varphi)$. All these parameters must be measured in order to obtain a reliable measurement of quarkonium polarization.

CMS has measured the polarizations of J/ψ, ψ(2S) [15] and of $\Upsilon(1S), \Upsilon(2S), \Upsilon(3S)$ [16, 17] at $\sqrt{s}$ = 7 TeV. The full angular decay distributions have been measured in three commonly used polarization frames (Collin-Soper CS, centre-of-mass helicity HX, and perpendicular helicity PX) and frame-independently. Non-prompt charmonium contributions have been removed using pseudo-proper decay time measurements. The continuum background is estimated from the side-bands on both sides of the signal regions in the invariant mass distributions such as the ones shown in Fig. 7.

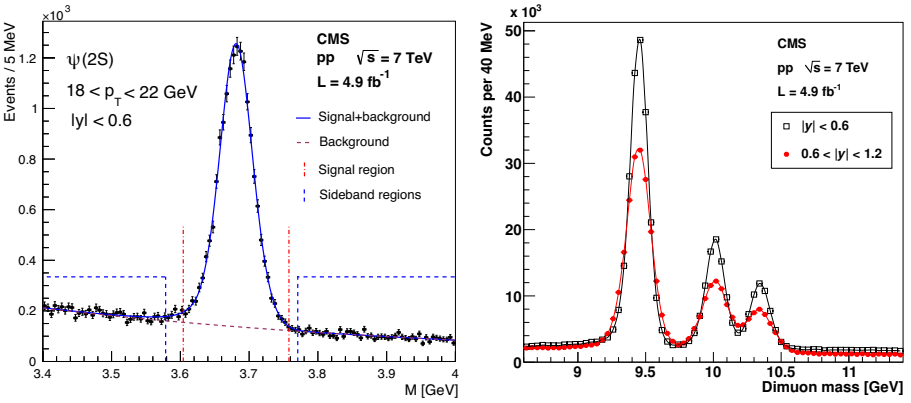

Figure 7. Invariant mass distributions for (Left) ψ(2S), (Right) $\Upsilon(1S), \Upsilon(2S), \Upsilon(3S)$.

As can be seen from Fig. 8 for J/ψ and ψ(2S), no strong polarization has been found, independently of p_T or y.

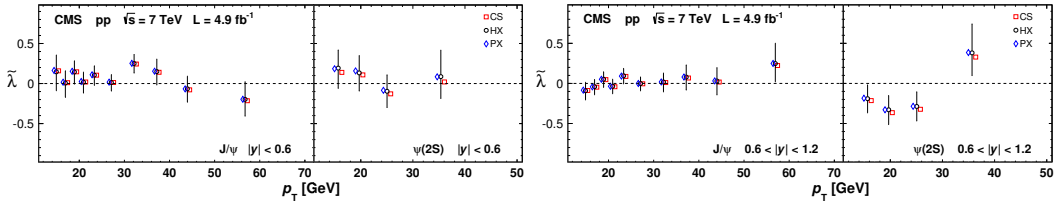

Figure 8. Polarization parameter $\tilde{\lambda}$ as a function of p_T for J/ψ and ψ(2S) in different rapidity regions.

The same is true for ϒ(nS), as depicted in Fig. 9, which shows also results from CDF.

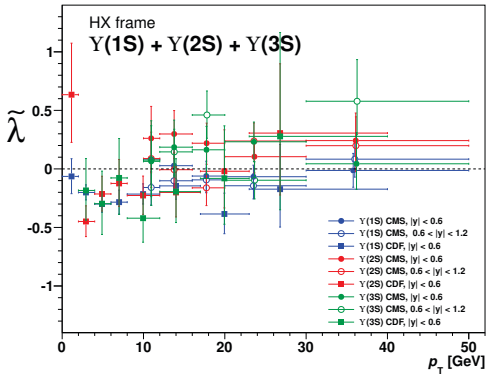

Figure 9. Polarization parameter $\tilde{\lambda}$ as a function of p_T for $\Upsilon(1S), \Upsilon(2S), \Upsilon(3S)$ in different rapidity regions, including results from CDF.

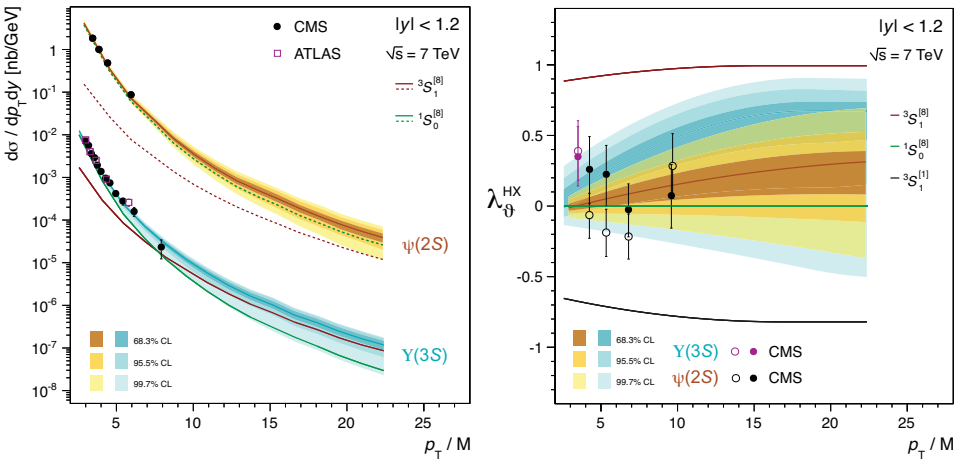

Figure 10. Mass-scaled distributions for $\psi(2S)$ and $\Upsilon(3S)$ (Left) diifferential cross sections, (Right) polarization parameter λ_θ in the HX frame.

A theory for quarkonium production is non-relativistic quantum chromodynamics (NRQCD), an effective field theory that has two factorized steps, the perturbative production of the initial quark-antiquark pair and the non-perturbative hadronization of the quark pair into a bound quarkonium state. NRQCD predicts the existence of intermediate color-octet (CO) states, which subsequently evolve into physical color-singlet (CS) quarkonia by the emission of soft gluons. S-wave vector quarkonia may be formed from heavy quark-antiquark pairs created as CS ($^3S_1^{[1]}$) or one of three color octets ($^1S_0^{[8]}, ^3S_1^{[8]}, ^3P_J^{[8]}$). NRQCD calculations at next-to-leading order (NLO) have been performed and compared with data.

Fig. 10 shows ATLAS and CMS measurements of the double-differential cross sections and the λ_ϑ polarization parameter in the HX frame as a function of p_T, mass-rescaled to equalize kinematic effects of different average parton momenta and phase spaces [18]. Extrapolations to higher p_T values than the ranges covered by the fitted data are made. Although χ_b(3P) feed-down contributions to Υ(3S) are neglected, it can be seen that no strong polarization is present and that the unpolarized ${}^1S_0^{[8]}$ component dominates quarkonium production.

Acknowledgments

I am grateful to my CMS colleagues, in particular Carlos Lourenço, Valentin Knünz, Ilse Krätschmer, and Nuno Viegas Guerreiro Leonardo, for their contributions.

References

[1] CMS Collaboration, JINST **3**, S08004 (2008)
[2] M. Butenschön, B. A. Kniehl, PRL **106**, 022003 (2011)
[3] J. Charles et al., PRD **84**, 033005 (2011)
[4] A. Lenz and U. Nierste, Proceedings of the 6th International Workshop on the CKM Unitarity Triangle, University of Warwick, UK, 6-10 Sep. 2010, arXiv:1102.4274
[5] CMS Collaboration, CMS-PAS BPH-13-012 (2013)
[6] A. S. Dighe, I. Dunietz, H. J. Lipkin, and J. L. Rosner, PLB **369**, 144 (1996)
[7] LHCb Collaboration, PRD **87**, 112010 (2013)
[8] http://www.slac.stanford.edu/xorg/hfag/
[9] CMS Collaboration, CMS-PAS BPH-14-001 (2014)
[10] P. Faccioli et al., JHEP **10**, 004 (2008)
[11] CMS Collaboration, PLB **727**, 381 (2013)
[12] CMS Collaboration, PRL **110**, 081802 (2013)
[13] CMS Collaboration, EPJC **71**, 1575 (2011)
[14] P. Faccioli et al., EPJC **69**, 657 (2010)
[15] CMS Collaboration, PLB **727**, 381 (2013)
[16] CMS Collaboration, PRL **108**, 151802 (2012)
[17] CMS Collaboration, PRL **110**, 081802 (2013)
[18] P. Faccioli et al., PLB **736**, 98 (2014)